Evaluation of Small-Molecule Modulators of the Luteinizing Hormone/Choriogonadotropin and Thyroid Stimulating Hormone Receptors: Structure−Activity Relationships and Selective Binding Patterns

Susanna Moore,[†,‡,§] Holger Jaeschke,[‡,#,§] Gunnar Kleinau,[||,⊥,§] Susanne Neumann,[‡] Stefano Costanzi,[||] Jian-kang Jiang,[†] John Childress,[‡] Bruce M. Raaka,[‡] Anny Colson,[||] Ralf Paschke,[#] Gerd Krause,[⊥] Craig J. Thomas,[†] and Marvin C. Gershengorn*[,‡]

Chemical Biology Core Facility, Clinical Endocrinology Branch, and Computational Chemistry Core Laboratory, National Institute of Diabetes and Digestive and Kidney Diseases, National Institutes of Health, Bethesda, Maryland 20892, III Department of Medicine, University of Leipzig, D-04103 Leipzig, Germany, and Structural Bioinformatics and Molecular Design, Leibniz-Institut für Molekulare Pharmakologie, D-13125 Berlin, Germany

Received March 3, 2006

The substituted thieno[2,3-*d*]pyrimidine **3** (Org 41841), a partial agonist for the luteinizing hormone/choriogonadotropin receptor (LHCGR) and the closely related thyroid-stimulating hormone receptor (TSHR), was fundamentally altered, and the resulting analogues were analyzed for their potencies, efficacies, and specificities at LHCGR and TSHR. Chemical modification of the parent compound combined with prior mutagenesis of TSHR provided compelling experimental evidence in support of computational models of **3** binding to TSHR and LHCGR within their transmembrane cores. Biochemical analysis of a specific modification to the chemical structure of **3** provides additional evidence of a H-bond between the ligand and a glutamate residue in transmembrane helix 3, which is conserved in both receptors. Several key interactions were surveyed to determine their respective biochemical roles in terms of both van der Waals dimensions and hydrogen bond capacity and the respective relationship to biological activity.

Introduction

Luteinizing hormone/choriogonadotropin (LH/CG), follicle-stimulating hormone (FSH), and thyroid-stimulating hormone (TSH) are heterodimeric glycoprotein hormones that regulate reproduction and thyroid homeostasis.[1−3] LH is responsible for ovulation induction in women and controls testosterone production in men. FSH causes ovarian follicle maturation in women and is involved in spermatogenesis in men. TSH is involved in the growth and function of thyroid follicular cells. Cellular responses to all three glycoprotein hormones are mediated via distinct seven transmembrane-spanning receptors (7-TMRs), i.e., the LHCGR, FSHR, and TSHR. Each receptor is characterized by an elongated extracellular domain distinguished by several leucine-rich motifs that are involved in recognition and binding of the large glycoprotein hormones. The seven-transmembrane helices of each receptor are noteworthy because of their high degree of homology.

Disruption of physiological regulation of LHCGR, FSHR, and TSHR by diverse pathogenic mutations has been implicated in a number of human diseases.[1,4] The specific and potent control of these multifunctioning receptors could provide important therapeutic advancements. LH and FSH are currently used clinically for the treatment of infertility, and it can be reasoned that synthetic agonists of LHCGR and FSHR have potential as infertility therapeutics. Recombinant TSH is used in the diagnostic screen for thyroid cancer. TSHR agonists and antagonists may well have utility in the diagnosis and treatment of thyroid cancer, respectively. The development of small-molecule modulators of LHCGR and FSHR has also been pursued with varying degrees of success.[5] Notable is the development of a FSHR antagonist **1**,[6] a FSHR agonist **2**,[7] and the potent LHCGR agonist **3**[8] (Org 41841) (Figure 1).

The advancement of low molecular weight modulators of 7-TMR function is well established within medicinal chemistry and pharmacology. While highly potent small-molecule agonists and antagonists of a multitude of 7-TMRs are frequently reported from high-throughput screening, their receptor specificity and binding mechanism often remains unknown. While the prohibitive number of 7-TMRs and other cellular targets preclude knowing the absolute specificity of any small molecule, the competitive interactions of pharmacologically active agents at highly homologous receptors can and should be explored. Moreover, when possessing a combination of data regarding the putative binding site of a pharmacological agent and a modest degree of structural information of homologous receptors, it may be possible to re-engineer the molecular structure of a known binding agent to alter the binding preference. Using a combination of molecular modeling and evaluation of the binding of **3** within several TSHR/LHCGR chimera mutants, we have recently reported that **3** was found to bind within the seven-transmembrane domain of the TSHR and LHCGR.[9] Specifically, **3** was shown to bind within a localized pocket between transmembrane helices 3−7 and extracellular loop 2. Low molecular weight ligands of the LHCGR and TSHR are remarkable in that they are not likely to compete with the large native hormones for binding at the extracellular N-terminal domain. Herein, we report the exploration of the small-molecule agonist **3** via several fundamental structural alterations and the

* To whom correspondence should be addressed. Phone and fax: 301-496-4128. E-mail: marving@intra.niddk.nih.gov.
† Chemical Biology Core Facility, National Institute of Diabetes and Digestive and Kidney Diseases.
‡ Clinical Endocrinology Branch, National Institute of Diabetes and Digestive and Kidney Diseases.
§ These authors contributed equally to this work.
# University of Leipzig.
|| Computational Chemistry Core Laboratory, National Institute of Diabetes and Digestive and Kidney Diseases.
⊥ Leibniz-Institut für Molekulare Pharmakologie.

10.1021/jm060247s CCC: $33.50
Published on Web 05/24/2006

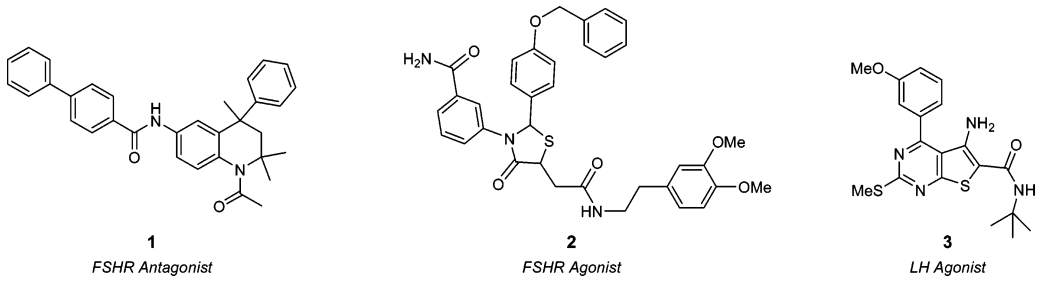

Figure 1. Structures of FSHR antagonist **1**, FSHR agonist **2**, and LHCGR agonist **3** (Org 41841).

Scheme 1[a]

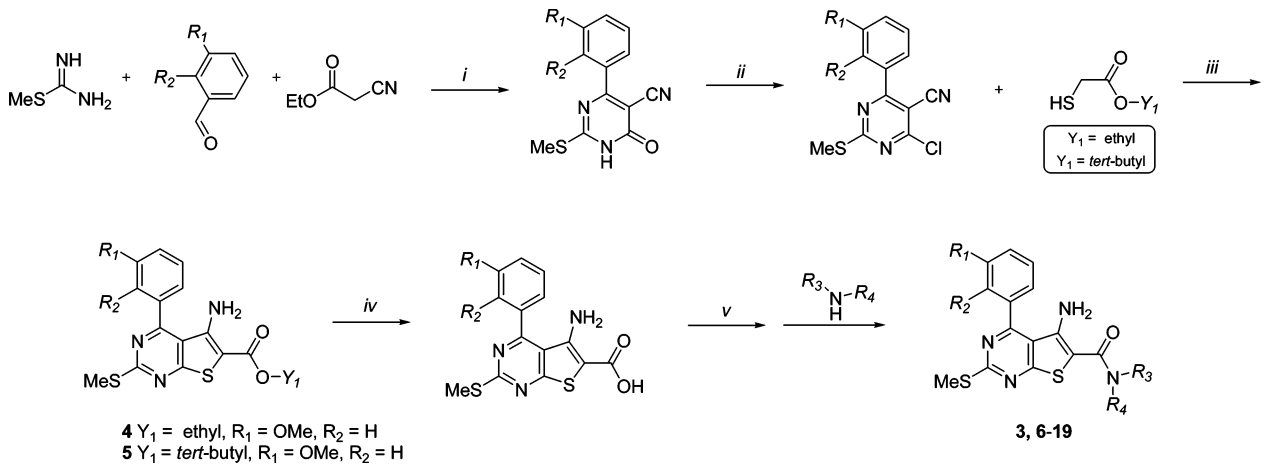

[a] Reagents and conditions: (i) K_2CO_3, EtOH, 60 °C, 5 h; (ii) $POCl_3$, dioxane, reflux, 2 h; (iii) NaOEt, EtOH, 50 °C, 3 h; (iv) LiOH, dioxane/H_2O; (v) PyBop, DIPEA, DMF followed by addition of amine (a subsequent benzyl deprotection was needed for the synthesis of analogue **19**; see Supporting Information).

resulting effects on efficacy, potency, and specificity between the highly homologous LHCGR and TSHR.

Results

Chemistry. The synthesis of **3** and several analogues based thereupon was accomplished in a manner similar to that described in the original report by van Boeckel and co-workers.[8] A modified Biginelli condensation afforded the substituted pyrimidone scaffold.[10] We found that numerous aldehydes were tolerated within this system including highly electron-withdrawn (i.e. polyfluoro and nitro) and electron-rich (polymethoxy and hydroxyl) aromatic ring systems. Treatment with $POCl_3$ afforded the 4-chloro-substituted pyrimidines in quantitative yields, and substitution with either ethyl 2-mercaptoacetate or *tert*-butyl 2-mercaptoacetate[11] afforded several thienopyrimidines, including biochemically relevant compounds **4** and **5** (Scheme 1). Saponification of the ethyl esters with lithium hydroxide in a dioxane/water mixture provided the thienopyrimidine acids, and PyBOP catalyzed amide couplings with several amines provided **3** and compounds **6**−**19**.[12]

Initial docking experiments suggested a potential hydrogen bond between the amine functionality of **3** and E3.37 in transmembrane helix 3 of both TSHR and LHCGR. To fully examine this, we chose to eliminate this potential interaction via two distinct experimental means. When the small molecule is used as a point of manipulation, the removal of the aromatic amine or the protection of the aromatic amine via dimethylation would accomplish the exclusion of H-bond donation capability. Unfortunately, all attempts to deaminate the structure of **3** were unsuccessful. However, direct treatment with methyl iodide in basic acetonitrile afforded the dimethylamine analogue **20** (Figure 2) along with the monomethylated and trimethylated analogues that were not characterized fully. Purification via HPLC was required prior to biological evaluation of **20**.

Biochemistry. Both human TSHR and human LHCGR were stably expressed in HEK 293 EM cells as previously described.[13,14] Cell surface expression of TSHR and LHCGR were determined via FACS analysis.[15] Agonism of compounds **3**−**20** were determined via measurement of intracellular cyclic AMP accumulation. It should be noted that **3** and the derivatives described herein were evaluated at the FSHR and no significant activity was observed.

Docking experiments of the ligand within both LHCGR and TSHR consistently suggested a potential hydrogen bond between the amine functionality of **3** and E3.37. We have previously reported the examination of this prospective interaction via an E to A mutant at position 3.37 for TSHR.[9] Consistent with the suggested interaction displayed in our models, E3.37A was not activated by **3**. The dimethylated analogue **20** provided a reagent to test this hypothesis directly by eliminating the needed hydrogen bond donation by the relevant amine. The resulting agonism displayed by **20** was shown to be only 7% relative to that of **3** at both LHCGR and TSHR (Figure 2). These experiments provide congruent evidence from two unrelated analyses for a critical H-bond between **3** and TSHR and LHCGR.

The chemical structure of **3** was further modified in a variety of ways in an attempt to define novel activity. Table 1 presents a compilation of the activities of **3**−**19**. Of note is the greater tolerance toward ligand modification found at the LHCGR compared to TSHR. To more adequately appreciate the differences in the receptor−ligand interaction, the full dose−response curves of **3**, **5**, and **7** were established (Figure 3). These analogues were chosen on the basis of the range of activation that was initially noted for each small molecule at both receptors. Further, each compound represents single-point alterations to the potentially important amide pharmacophore. These experiments show that the addition of an *N*-methyl group to the *tert*-

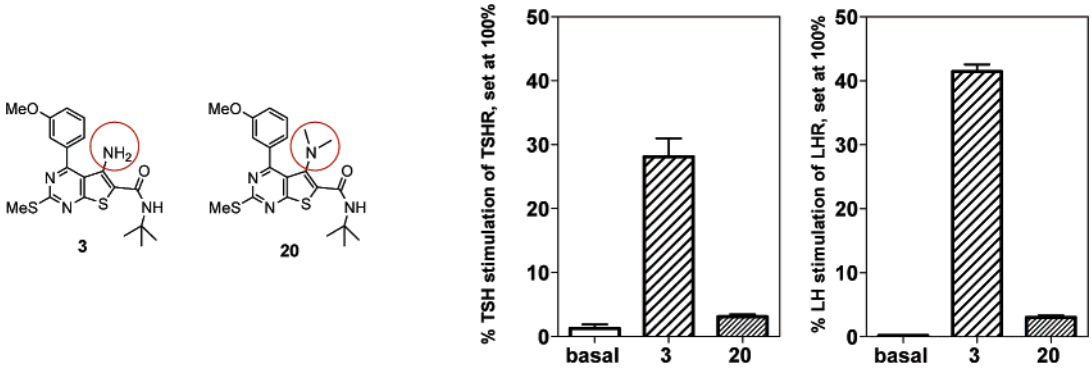

Figure 2. Analysis of **20** at both the TSHR and LHCGR. Comparison of the activation of TSHR and LHCGR by compounds **3** and **20** relative to basal activities of both receptors is shown. Intracellular cAMP production was determined in response to 100 μM of each compound and is expressed as the percent of maximum response of TSHR/LHCGR to TSH (100 mU/mL)/LH (1000 ng/mL). The data are presented as the mean ± SEM of two independent experiments, each performed in duplicate.

Table 1. Pharmacological Characterization of Selected Analogues of **3** at TSHR and LHCGR Stably Expressed in HEK EM 293 Cells[a]

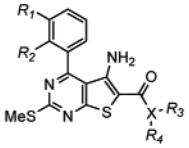

Analogue #	X	R_1	R_2	R_3	R_4	EC_{50} (LHCGR) in μM [95% C. I.]	% Max. Resp. @ LHCGR in μM	EC_{50} (TSHR) in μM [95% C. I.]	% Max. Resp. @ TSHR in μM
3	N	OMe	H	*t*Bu	H	0.3 [0.2 - 0.5]	45.8 ± 5.9	6.5 [4.9 - 8.5]	23.4 ± 3.6
4	O	OMe	H	Et	H	n.d.	4.2 ± 2.2	n.d.	1.5 ± 0.2
5	O	OMe	H	*t*Bu	H	1.1 [0.8 - 1.5]	23.8 ± 3.3	11.9**	> 30.3*
6	N	OMe	H	Et	H	n.d.	26.9 ± 4.8	n.d.	2.3 ± 0.4
7	N	OMe	H	*t*Bu	Me	0.8 [0.6 - 1.2]	47.8 ± 2.8	n.d.	3.6 ± 1.9
8	N	OMe	H	NH_2	H	n.d.	8.5 ± 3.6	n.d.	6.1 ± 0.8
9	N	OMe	H	$N(Me)_2$	H	n.d.	11.0 ± 1.5	n.d.	4.0 ± 0.1
10	N	OMe	H	NH(*t*Bu)	H	n.d.	6.0 ± 3.1	n.d.	6.4 ± 0.6
11	N	OMe	H	NH(Boc)	H	n.d.	2.4 ± 0.5	n.d.	1.9 ± 0.4
12	N	OMe	H		H	n.d.	20.5 ± 2.7	n.d.	2.9 ± 0.5
13	N	OMe	H		H	n.d.	20.3 ± 2.1	n.d.	3.6 ± 0.6
14	N	OMe	H		H	n.d.	7.8 ± 2.7	n.d.	3.0 ± 1.2
15	N	OMe	H		H	n.d.	25.6 ± 5.4	n.d.	4.3 ± 0.4
16	N	OMe	OMe	*t*Bu	H	0.8 [0.7 - 1.0]	50.1 ± 3.6	n.d.	3.0 ± 0.9
17	N	OMe	F	*t*Bu	H	1.5 [1.0 - 2.1]	46.3 ± 6.6	11.5**	> 24.0*
18	N	F	H	*t*Bu	H	1.2 [0.8 - 1.6]	51.1 ± 5.2	n.d.	8.1 ± 1.7
19	N	OH	H	*t*Bu	H	1.9 [1.1 - 3.4]	63.9 ± 14.2	n.d.	11.2 ± 1.0

[a] Agonistic activity of compounds was determined via measurement of intracellular cyclic AMP. The efficacy (maximum response) is expressed as the percent of maximum response of LHCGR or TSHR to LH (1000 ng/ml) or TSH (100 mU/mL), respectively. EC_{50} values and 95% conficence intervals (C.I.) were obtained from dose−response curves (0−100 μM compound) using the GraphPad Prism 4.0 software. Confidence intervals were not calculated in dose−response curves that did not reach an obvious plateau. n.d. = not determined. ∗ = estimated maximum response at 100 μM compound. ∗∗ = estimated EC_{50} (dose−response curve revealed no plateau).

butylamide in compound **7** precludes an agonistic response at the TSHR while allowing a response at LHCGR similar to that of **3**. The original report of **3** described the utility of the *tert*-butyl moiety as a major determinant of its potency at LHCGR. We explored the role of the linkage (amide or ester) between the aromatic and *tert*-butyl segments of **3**. The alteration of the *tert*-butylamide (displayed in **3**) to a *tert*-butyl ester (displayed in **5**) had a deleterious effect on both potency and efficacy at LHCGR, while the activity at TSHR was unaffected.

Docking Studies. We have previously reported the construction of molecular models of TSHR and LHCGR.[9] In this study, by means of the ICM software,[16] **3** and selected analogues were docked within the previously described binding pockets of **3** at TSHR and LHCGR (detailed experimental procedures and descriptions are found in the Supporting Information).[9]

The similarities and dissimilarities of the amino acid residues between the receptor subtypes were studied to elucidate positions that form and cover the binding pocket for the two receptors. To facilitate the comparative relationship between selected residues of each receptor, a GPCR residue indexing system was utilized (i.e., E3.37 for E506 at TSHR and for E451 at LHCGR).[17,18] Several conserved amino acids, such as the key glutamate (E3.37), as well as nonconserved amino acids, such as the F → T (position 5.42), Y → F (position 6.54) and L → F (position 570/515), were deemed relevant toward the binding of **3** at both LHCGR and TSHR. A complete comparison of

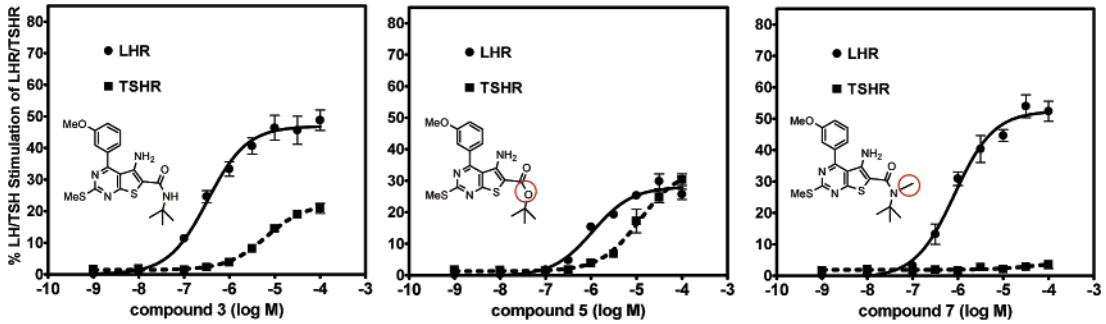

Figure 3. Full concentration analyses of compounds **3**, **5**, and **7** at TSHR and LHCGR. The data are presented as the mean ± SEM of two independent experiments, each performed in duplicate.

Table 2. Comparison of Selected Amino Acid Residues of the TSHR and LHCGR with Relevance to the Org 41841 Binding Pocket

region	position	TSHR	LHCGR
TMH3	3.32	Thr 501	Thr 446
	3.33	Val 502	Val 447
	3.36	Ser 505	Ser 450
	3.37	Glu 506	Glu 451
	3.40	Val 509	Val 454
TMH 4	**4.56**	**Leu 552**	**Ile 497**
	4.57	Ala 553	Ala 498
	4.59	Leu 555	Leu 500
	4.60	Pro 556	Pro 501
ECL 2		**Ile 560**	**Val 505**
		Ser 561	Ser 506
		Leu 570	**Phe 515**
		Pro 571	Pro 516
		Met 572	Met 517
		Asp 573	Asp 518
TMH 5	**5.34**	**Pro 577**	**Thr 522**
	5.36	**Ala 579**	**Ser 524**
	5.37	**Leu 580**	**Gln 525**
	5.38	**Ala 581**	**Val 526**
	5.39	Tyr 582	Tyr 527
	5.42	**Phe 585**	**Thr 530**
	5.43	**Val 586**	**Ile 531**
	5.46	Leu 589	Leu 534
	5.47	Asn 590	Asn 535
TMH 6	6.48	Met 637	Met 582
	6.51	Ile 640	Ile 585
	6.52	Ser 641	Ser 586
	6.54	**Tyr 643**	**Phe 588**
	6.55	Ala 644	Ala 589
	6.59	**Ile 648**	**Ala 593**
TMH 7	7.39	Val 664	Val 609
	7.42	Tyr 667	Tyr 612

[a] Amino acids are identified according to the residue numbering (including signal peptide) and to the Ballesteros−Weinstein numbering. The binding pockets of TSHR and LHCGR are composed of 32 amino acids, 11 of which are divergent. TMH = transmembrane helix. ECL = extracellular loop. Bolded residues indicate dissimilar amino acid residues.

the amino acid residues that form the putative binding pockets is shown in Table 2.

The resulting models represent an extension of our previous work on TSHR[9,15] and constitute the first reported docking models of this class of ligands at LHCGR. In part, the models confirm our supposition that LHCGR contains a larger binding pocket than the TSHR. This has numerous consequences with regard to the binding mode of **3** and selected analogues within the two related receptors. From an early stage in our modeling experiments it was apparent that **3** could bind in two distinct orientations in both receptors with nearly similar docking scores. Common to both is the pivotal role of E3.37 as a hydrogen bond acceptor. Further, these two orientations were statistically more significant than all other docking orientations examined. They can be briefly explained by using the methoxyphenyl moiety as a point of reference. In orientation A, the methoxyphenyl ring is seen in a position proximal to transmembrane helixes 4 and 5 and bordering the extracellular loop region. In orientation B, the methoxyphenyl ring is seen in a position proximal to transmembrane helix 3 and more deeply buried within the transmembrane core (Figure 4). We chose to amplify upon these two orientations by docking selected analogues of **3** (namely, compounds **5** and **7**) based on the altered hydrogen bond capacity of the amide and their differing pharmacological results. We further anticipated that the docking models would allow us to amplify upon the relevance of the *tert*-butylamide moiety in terms of both van der Waals dimensions and hydrogen bond capacity. Both binding orientations for both receptors (shown in Figure 4 for **3** and in the Supporting Information for **5** and **7**) are shared (with certain dissimilarities) for all three compounds.

A detailed survey of the resulting 12 models (shown in the Supporting Information) provided several points of interest but none more striking than the significant docking shifts that were noted for analogue **7** (Figure 5). Despite bearing a larger and more hindered amide substituent because of the presence of an additional methyl group, compound **7** can be accommodated within the binding pocket of LHCGR with direct overlap with compound **3**. In contrast, in molecular models of the TSHR, the larger van der Waals dimensions of compound **7** did *not* allow this compound to adopt a docking pose similar to that of **3** in either orientation A or B (Figure 5 details the docking of **7** in orientation A). Because of the additional steric constraints, the amide moiety of compound **7** could not be accommodated in the tightly packed region surrounding M6.48 in orientation A within the TSHR and, importantly, the essential H-bond with E3.37 was not observed. Moreover, the increased bulkiness of the amide moiety of compound **7** generated a steric clash within the TSHR binding pocket of orientation B as well. Further, fewer docking poses with acceptable docking scores were observed for **7** within TSHR molecular models presumably because of the presence of the bulkier amino acid residues that constitute the binding pocket (i.e., L570, F5.42, and I6.59). Consequently, the aromatic amine moiety of compound **7** did not engage in a H-bond with E3.37 (the distance between carboxyl oxygen of E3.37 and the NH_2 group of compound **7** was noted to be 5.7 Å, shown in Supporting Information). These results are significant for the advancement of next-generation derivatives of **3**.

Discussion

The optimization of the binding arrangements of **3** within the molecular models of LHCGR and TSHR provided numerous insights that could be experimentally examined. For instance, we determined whether exploitation of the T → F variation (T530 and F585 in LHCGR and TSHR, respectively) could provide an analogue of **3** with altered specificity favoring TSHR activation. To this end we synthesized several aromatic amides

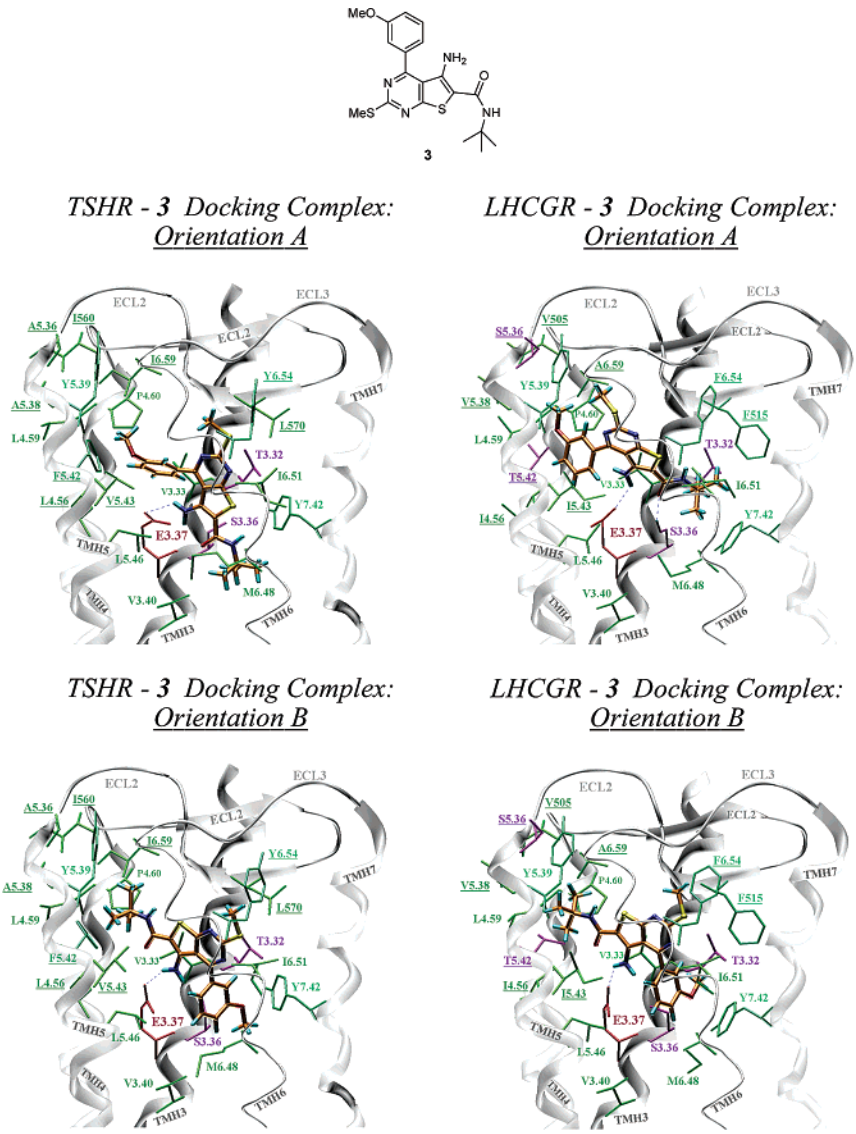

Figure 4. Docking poses of **3** within homology models of TSHR and LHCGR optimized to orientations A and B. The binding pocket is located within the extracellular half of the transmembrane helical bundle between TMH 3−7 and ECL 2 (backbone ribbons in white). Amino acids that are not conserved between the two receptors are underlined. Coloring is as follows: green = hydrophobic side chains; green/blue = aromatic side chains; magenta = hydrophilic side chains; red = negatively charged side chains. Compound **3** is shown in orange with atoms in color.

(**14** and **15**) in the hope of achieving a stacking interaction between the phenyl rings of the altered compounds and F585. There was, however, no enhancement of activity at TSHR based on these structural modifications to **3**. We also took note of the specific interactions between **3** and the negatively charged E3.37 and synthesized several analogues with amplified positive charge and/or enhanced H-bonding capacity in an effort to enhance the binding of the small molecule. However, none of these derivatives (**8**−**11**) were found to be effective modulators of either receptor. Several derivatives were synthesized in an effort to introduce functionality with different H-bonding capacity at the amide portion of the molecule (**12** and **13**) in the hopes of defining novel binding arrangements for receptor activation. However, neither derivative provided an enhancement of potency or selectivity. Our studies did confirm that the *tert*-butyl moiety was optimal for the small molecule to interact with one of the two hydrophobic cores (between TMH4 and TMH5 proximal to the extracellular domain and between TMH3 and TMH6 near the M6.48 region) located within the binding pocket defined by our models. Further, the necessity of the amide functionality was confirmed by the distinct activities of **3** and **5**. We are unable, on the basis of our current experiments and models, to categorize the amide pharmacophore from the basis of the H-bond variance of amides and esters or the associated van der Waals constraints. A small survey of the methoxyphenyl ring revealed that modest alterations of this moiety are seemingly allowed. In particular, the replacement of the methoxy group with a hydroxyl (**19**) was noted to have no critical influence on the potency at the LHCGR but a large enhancement in the displayed efficacy.

Analysis of the docking models of this class of ligands at both LHCGR and TSHR provided two distinct docking orientations. The two orientations have nearly equivalent docking scores, and yet they represent two vastly divergent ligand postures. It should be noted that recent structural modifications of **3** have denoted that the methoxyphenyl ring can be modified to accommodate larger substitutions (such as phenylamide and several small peptide chains up to eight atoms) without consequence toward the potency of the small molecule at the LHCGR.[5] Taking these data into account does not provide any definitive preference in favor of either orientation A or B, since the limited spatial extension at the methoxy moiety was

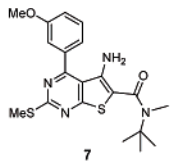

7

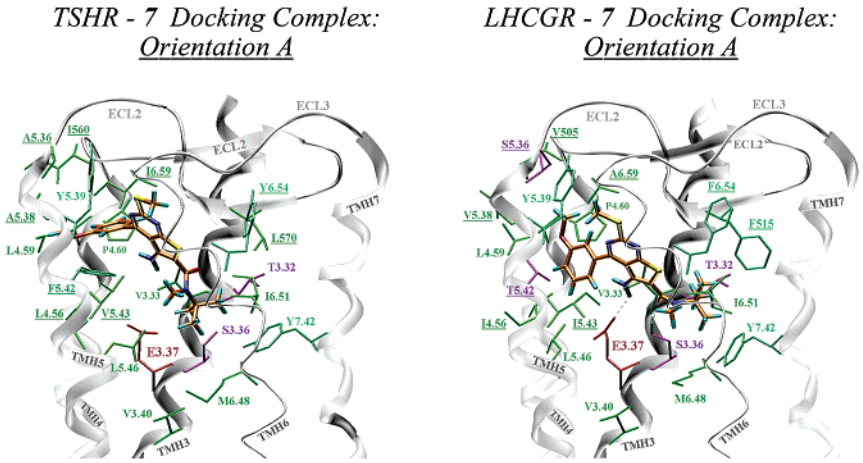

Figure 5. Docking pose of **7** within homology model of TSHR optimized to orientation A. The binding pocket is located within the extracellular half of the transmembrane helical bundle between TMH 3−7 and ECL 2 (backbone ribbons in white). Amino acids that are not conserved between the two receptors are underlined. Coloring is as follows: green = hydrophobic side chains; green/blue = aromatic side chains; magenta = hydrophilic side chains; red = negatively charged side chains. Compound **7** is shown in orange with atoms in color.

accommodated in both cases. From Figure 4 (right) one can comprehend that in orientation A limited spatial extension such as the phenylamide are spatially feasible at Y5.39 in the LH/CGR. In orientation B a phenylamide could be accommodated above Y7.42 between TMH7 and TM3.

The predicted interaction best supported by experimental data is the H-bond observed between the amine functionality of **3** and E3.37. We examined this potential interface by converting the amine to a dimethylamine moiety in **20**, thus eliminating the H-bond donation capacity of the small molecule (Figure 2). Previously, we mutated TSHR to eliminate the glutamate residue and thus abolish the H-bond potential between the receptor and the small molecule.[9] We observed that each of these independent changes markedly reduced agonistic activity at TSHR and, in terms of the activity of **20**, at LHCGR as well. This provides compelling experimental evidence supporting the existence of a critical H-bond between the small molecule and E3.37 and our proposed molecular docking arrangements of **3** within both LHCGR and TSHR.

Among the most important derivatives of the parent compound was the *N*-*tert*-butyl-*N*-methyl analogue **7**. This small molecule was noted to retain similar potency and efficacy at LHCGR while, importantly, eliminating the modest activity displayed by **3** at TSHR. Examination of **7** within our TSHR docking studies revealed that the slight addition of steric bulk at the amide was sufficient to eliminate the apparently critical H-bond between the compound and E3.37. However, docking of **7** within our LHCGR homology models revealed good overlap with the parent compound and the apparently critical hydrogen bond is unaltered. Again, these results provide persuasive evidence for a putative binding pocket within a cleft between transmembrane helices 3−6 of both receptors.

Conclusion

Herein, we have described the first reported docking model of a LHCGR−small molecule complex. Further, we have refined our model of the highly homologous TSHR−small molecule complex and compared the two models in an attempt to identify a mechanism by which the selectivity of **3** could be optimized. Several fundamental adjustments were made to the scaffold of **3** in an attempt to take advantage of several key amino acid residue variances between the two receptors. A critical hydrogen bond between **3** and a key glutamate residue (E3.37) was suggested by molecular modeling and subsequently confirmed by complementary experimental evidence through mutagenesis of the receptor target[9] and modification of the small-molecule ligand. The selectivity of **3** toward LHCGR was amplified by taking note of the smaller binding pocket within TSHR and accordingly increasing the steric bulk of the amide portion of the molecule (compound **7**). Modeling revealed a potential mechanism for this selectivity through the preclusion of the required H-bond to E3.37 based on the hindered interaction between **7** and TSHR. These results will be of key importance in improving our molecular model of the receptor−small molecule interaction and further refinement of the ligand.

Experimental Section

General. ^{1}H NMR data were recorded on a Varian Gemini 300 MHz instrument. Spectra were recorded in DMSO-d_6, $CDCl_3$-d_4, and acetone-d_6 and were referenced to the residual solvent peak at 2.50, 7.26 and 2.04 ppm, respectively. Reverse-phase (C18) HPLC was carried out using an Agilent HPLC with a Zorbax SP-C18 semiprep column. High-resolution mass spectrometry measurements were performed on a Micromass/Waters LCT Premier electrospray TOF mass spectrometer.

General Experimental Procedures. 5-Carbonitrile-1,6-dihydro-2-(methylthio)-6-oxo-4-(substituted phenyl)pyrimidines. To a solution of *S*-methylisothiourea (1 equiv), the appropriately substituted benzaldehyde (2 equiv) and ethyl cyanoacetate (2 equiv) in ethanol was added K_2CO_3 (2 equiv). The reaction mixture was heated to 60 °C for 5 h and filtered upon cooling to obtain products. Purification by flash chromatography (using EtOAc/hexane 1:1) provided the final products as off-white solids in 30−50% yields.

5-Carbonitrile-4-chloro-2-(methylthio)-6-(3-substituted phenyl)pyrimidines. To a mixture of the oxopyrimidines in dioxane was added $POCl_3$ (excess) in dioxane. The mixture was heated to reflux for 3 h, and the solvent was removed by reduced pressure.

Saturated $NaHCO_3$ was added to the resulting brown solids, and the reaction mixtures were extracted with CH_2Cl_2 (3 × 100 mL). The organic layers were combined and dried over Na_2SO_4, and the solvent was removed under reduced pressure. Purification by silica plug filtration (using EtOAc/hexane 1:1) provided the final products as white crystalline solids in 80−90% yields.

Ethyl 5-Amino-2-(methylthio)-4-(substituted phenyl)thieno-[2,3-*d*]pyrimidine-6-carboxylates. To a solution of the appropriate pyrimidine (1 equiv) and ethyl 2-mercaptoacetate or *tert*-butyl-2-mercaptoacetate (1.1 equiv) in ethanol was added sodium (0.910 equiv) in ethanol. The yellow reaction mixture was heated to 50 °C for 3 h and cooled, and the ethanol was removed under reduced pressure. The yellow solids were dissolved in CH_2Cl_2 (50 mL) and washed with deionized water (3 × 25 mL). The organic layer was dried over Na_2SO_4, and the solvent was removed under reduced pressure. Purification by flash chromatography (using EtOAc/hexane 1:1) provided the final products as yellow solids in 70−90% yields.

***N*-*tert*-Butyl-5-amino-2-(methylthio)-4-(substituted phenyl)-thieno[2,3-*d*]pyrimidine-6-carboxamides.** To a solution of the appropriate ethyl ester (1 eqiuv) in a dioxane and water mixture was added lithium hydroxide (2 equiv). The reaction mixture was heated to 50 °C for 3 h and cooled, and the solvent was removed under reduced pressure. The crude acid was used without further purification. The yellow solids were dissolved in a minimal amount of DMF, followed by the addition of PyBOP (3 equiv), DIPEA (5.5 equiv), and *tert*-butylamine (3 equiv), sequentially. Purification by flash chromatography (using EtOAc/hexane 2:1) provided the final products as yellow solids in 50−90% yields.

***N*-*tert*-Butyl-5-amino-4-(3-methoxyphenyl)-2-(methylthio)-thieno[2,3-*d*]pyrimidine-6-carboxamide (3).** Analysis by C_8 reversed-phase LC−MS using a linear gradient of H_2O with increasing amounts of CH_3CN (0 → 17 min, 30% → 70% CH_3CN at a flow rate of 1 mL/min, t_R = 13.5 min) indicated greater than 99% purity by peak integration. ^1H NMR ($CDCl_3$) δ 1.45 (s, 9H), 2.64 (s, 3H), 3.86 (s, 3H), 5.99 (br s, 2H), 7.07−7.26 (m, 3H), 7.41−7.47 (m, 1H); mass spectrometry (TOF) m/z = 403.1262 (M + H^+) (theoretical 403.1257).

Ethyl 5-Amino-4-(3-methoxyphenyl)-2-(methylthio)thieno[2,3-*d*]pyrimidine-6-carboxylate (4). Analysis by C_8 reversed-phase LC−MS using a linear gradient of H_2O with increasing amounts of CH_3CN (0 → 15 min, 30% → 90% CH_3CN at a flow rate of 1 mL/min, t_R = 12.5 min) indicated greater than 92% purity by peak integration. ^1H NMR (DMSO-d_6) δ 1.37 (t, J = 7.2 Hz, 3H), 2.69 (s, 3H), 3.92 (s, 3H), 4.35 (q, J = 7.2 Hz, 2H), 6.15 (br s, 2H), 7.27−7.31 (m, 3H), 7.59−7.64 (m, 1H); mass spectrometry (TOF) m/z = 376.0790 (M + H^+) (theoretical 376.0784).

***tert*-Butyl 5-Amino-4-(3-methoxyphenyl)-2-(methylthio)thieno-[2,3-*d*]pyrimidine-6-carboxylate (5).** Analysis by C_8 reversed-phase LC−MS using a linear gradient of H_2O with increasing amounts of CH_3CN (0 → 15 min, 30% → 90% CH_3CN at a flow rate of 1 mL/min, t_R = 13.2 min) indicated greater than 98% purity by peak integration. ^1H NMR ($CDCl_3$) δ 1.57 (s, 9H), 2.64 (s, 3H), 3.86 (s, 3H), 5.78 (br s, 2H), 7.08−7.16 (m, 3H), 7.42−7.47 (m, 1H); mass spectrometry (TOF) m/z = 404.1097 (M + H^+) (theoretical 404.1103).

5-Amino-*N*-(ethyl)-4-(3-methoxyphenyl)-2-(methylthio)thieno-[2,3-*d*]pyrimidine-6-carboxamide (6). Analysis by C_8 reversed-phase LC−MS using a linear gradient of H_2O with increasing amounts of CH_3CN (0 → 18 min, 40% → 80% CH_3CN at a flow rate of 1 mL/min, t_R = 9.8 min) indicated greater than 99% purity by peak integration. ^1H NMR (DMSO-d_6) δ 1.08 (t, J = 7.2 Hz, 3H), 2.59 (s, 3H), 3.22 (p, J = 7.2 Hz, 2H), 3.82 (s, 3H), 5.75 (s, 1H), 6.10 (br s, 2H), 7.15−7.19 (m, 2H), 7.50 (t, J = 8.0 Hz, 1H), 7.87 (t, J = 8.0 Hz, 1H); mass spectrometry (TOF) m/z = 375.0944 (M + H^+) (theoretical 375.0949).

***N*-*tert*-Butyl-5-amino-4-(3-methoxyphenyl)-*N*-methyl-2-(methylthio)thieno[2,3-*d*]pyrimidine-6-carboxamide (7).** Analysis by C_8 reversed-phase LC−MS using a linear gradient of H_2O with increasing amounts of CH_3CN (0 → 18 min, 40% → 80% CH_3CN at a flow rate of 1 mL/min, t_R = 14.6 min) indicated greater than 95% purity by peak integration. ^1H NMR (DMSO-d_6) δ 1.36 (s, 9H), 2.58 (s, 3H), 3.00 (s, 3H), 3.82 (s, 3H), 5.22 (br s, 2H), 7.17−7.20 (m, 3H), 7.51 (t, J = 8 Hz, 1H); mass spectrometry (TOF) m/z = 417.1413 (M + H^+) (theoretical 417.1419).

5-Amino-4-(3-methoxyphenyl)-2-(methylthio)thieno[2,3-*d*]pyrimidine-6-carbohydrazide (8). Analysis by C_8 reversed-phase LC−MS using a linear gradient of H_2O with increasing amounts of CH_3CN (0 → 18 min, 40% → 80% CH_3CN at a flow rate of 1 mL/min, t_R = 13.7 min) indicated greater than 92% purity by peak integration. ^1H NMR (DMSO-d_6) δ 2.59 (s, 3H), 3.82 (s, 3H), 6.18 (br s, 2H), 7.17−7.20 (m, 3H), 7.50 (t, J = 8.7 Hz, 1H), 9.20 (br s, 1H); mass spectrometry (TOF) m/z = 362.074 (M + H^+) (theoretical 362.0745).

5-Amino-4-(3-methoxyphenyl)-*N*′,*N*′-dimethyl-2-(methylthio)-thieno[2,3-*d*]pyrimidine-6-carbohydrazide (9). Analysis by C_8 reversed-phase LC−MS using a linear gradient of 0.1% TFA in H_2O with increasing amounts of CH_3CN (0 → 18 min, 30% → 80% CH_3CN at a flow rate of 1 mL/min, t_R = 8.7 min) indicated greater than 93% purity by peak integration. ^1H NMR (DMSO-d_6) δ 2.55 (s, 6H), 2.58 (s, 3H), 3.82 (s, 3H), 6.45 (br s, 2H), 7.16−7.18 (m, 3H), 7.50 (t, J = 8.7 Hz, 1H), 8.72 (s, 1H); mass spectrometry (TOF) m/z = 390.1053 (M + H^+) (theoretical 390.1058).

***N*′-*tert*-Butyl-5-amino-4-(3-methoxyphenyl)-2-(methylthio)-thieno[2,3-*d*]pyrimidine-6-carbohydrazide (10).** Analysis by C_8 reversed-phase LC−MS using a linear gradient of H_2O with increasing amounts of CH_3CN (0 → 10 min, 25% → 90% CH_3CN, 10 → 15 min, 90% → 25% CH_3CN at a flow rate of 1 mL/min, t_R = 12.0 min) indicated greater than 95% purity by peak integration. ^1H NMR (DMSO-d_6) 1.08 (s, 9H), 2.59 (s, 3H), 3.82 (s, 3H), 6.45 (br s, 2H), 7.16−7.18 (m, 3H), 7.50 (t, J = 8 Hz, 1H); mass spectrometry (TOF) m/z = 418.1366 (M + H^+) (theoretical 418.1371).

***N*′-Boc-5-amino-4-(3-methoxyphenyl)-2-(methylthio)thieno-[2,3-*d*]pyrimidine-6-carbohydrazide (11).** Analysis by C_8 reversed-phase LC−MS using a linear gradient of H_2O with increasing amounts of CH_3CN (0 → 10 min, 25% → 90% CH_3CN, 10 → 15 min, 90% → 25% CH_3CN at a flow rate of 1 mL/min, t_R = 11.0 min) indicated greater than 97% purity by peak integration. ^1H NMR (DMSO-d_6) 1.42 (s, 9H), 2.60 (s, 3H), 3.82 (s, 3H), 6.18 (br s, 2H), 7.16−7.21 (m, 3H), 7.51 (t, J = 8 Hz, 1H), 8.83 (bs, 1H), 9.62 (bs, 1H); mass spectrometry (TOF) m/z = 462.1264 (M + H^+) (theoretical 462.127).

5-Amino-4-(3-methoxyphenyl)-*N*-(2-hydroxyethyl)-2-(methylthio)thieno[2,3-*d*]pyrimidine-6-carboxamide (12). Analysis by C_8 reversed-phase LC−MS using a linear gradient of H_2O with increasing amounts of CH_3CN (0 → 18 min, 30% → 60% CH_3CN at a flow rate of 1 mL/min, t_R = 7.4 min) indicated greater than 92% purity by peak integration. ^1H NMR (DMSO-d_6) δ 2.59 (s, 3H), 3.20−3.40 (m, 2H), 3.41−3.55 (m, 2H), 3.82 (s, 3H), 4.71 (m, 1H), 6.10 (br s, 2H), 7.17−7.22 (m, 3H), 7.50 (m, 1H), 7.80 (m, 1H); mass spectrometry (TOF) m/z = 391.0893 (M + H^+) (theoretical 391.0899).

5-Amino-*N*-(cyanomethyl)-4-(3-methoxyphenyl)-2-(methylthio)thieno[2,3-*d*]pyrimidine-6-carboxamide (13). Analysis by C_8 reversed-phase LC−MS using a linear gradient of H_2O with increasing amounts of CH_3CN (0 → 10 min, 25% → 90% CH_3CN, 10 → 15 min, 90% → 25% CH_3CN at a flow rate of 1 mL/min, t_R = 10.5 min) indicated greater than 91% purity by peak integration. ^1H NMR (DMSO-d_6) δ 2.60 (s, 3H), 3.82 (s, 3H), 4.22 (d, J = 5.4 Hz, 2H), 6.23 (br s, 2H), 7.18−7.20 (m, 3H), 7.51 (t, J = 8.1 Hz, 1H), 8.53 (t, J = 5.4 Hz, 1H); mass spectrometry (TOF) m/z = 386.074 (M + H^+) (theoretical 386.0745).

5-Amino-*N*-benzyl-4-(3-methoxyphenyl)-2-(methylthio)thieno-[2,3-*d*]pyrimidine-6-carboxamide (14). Analysis by C_8 reversed-phase LC−MS using a linear gradient of H_2O with increasing amounts of CH_3CN (0 → 18 min, 40% → 80% CH_3CN at a flow rate of 1 mL/min, t_R = 12.6 min) indicated greater than 99% purity by peak integration. ^1H NMR (acetone-d_6) δ 2.61 (s, 3H), 3.89 (s, 3H), 4.55 (d, J = 6 Hz, 2H), 6.29 (br s, 2H), 7.18−7.37 (m, 8H),

7.49 (t, $J = 8.4$ Hz, 1H), 7.64 (t, $J = 3$ Hz, 1H); mass spectrometry (TOF) $m/z = 437.1100$ ($M + H^+$) (theoretical 437.1106).

5-Amino-4-(3-methoxyphenyl)-2-(methylthio)-*N*-phenethylthieno[2,3-*d*]pyrimidine-6-carboxamide (15). Analysis by C_8 reversed-phase LC−MS using a linear gradient of H_2O with increasing amounts of CH_3CN (0 → 18 min, 40% → 80% CH_3CN at a flow rate of 1 mL/min, $t_R = 14.7$ min) indicated greater than 98% purity by peak integration. ^{1}H NMR (DMSO-d_6) δ 2.59 (s, 3H), 2.81 (t, $J = 7.2$ Hz, 2H), 3.43 (q, $J = 8.4$ Hz, 2H), 3.82 (s, 3H), 6.11 (br s, 2H), 7.16−7.32 (m, 8H), 7.50 (t, $J = 7.8$ Hz, 1H), 7.96 (t, $J = 3$ Hz, 1H); mass spectrometry (TOF) $m/z = 451.1257$ ($M + H^+$) (theoretical 451.1262).

***N*-*tert*-Butyl-5-amino-4-(2,3-dimethoxyphenyl)-2-(methylthio)-thieno[2,3-*d*]pyrimidine-6-carboxamide (16).** Analysis by C_8 reversed-phase LC−MS using a linear gradient of H_2O with increasing amounts of CH_3CN (0 → 16 min, 35% → 95% CH_3CN at a flow rate of 1 mL/min, $t_R = 14.3$ min) indicated greater than 93% purity by peak integration. ^{1}H NMR ($CDCl_3$) δ 1.45 (s, 9H), 2.66 (s, 3H), 3.76 (s, 3H), 3.95 (s, 3H), 5.77 (br s, 2H), 6.91 (dd, $J = 1.3$, 7.5 Hz, 1H), 7.21 (t, $J = 8.2$ Hz, 1H); mass spectrometry (TOF) $m/z = 433.1363$ ($M + H^+$) (theoretical 433.1368).

***N*-*tert*-Butyl-5-amino-4-(2-fluoro-3-methoxyphenyl)-2-(methylthio)thieno[2,3-*d*]pyrimidine-6-carboxamide (17).** Analysis by C_8 reversed-phase LC−MS using a linear gradient of H_2O with increasing amounts of CH_3CN (0 → 15 min, 35% → 90% CH_3CN at a flow rate of 1 mL/min, $t_R = 11.0$ min) indicated greater than 92% purity by peak integration. ^{1}H NMR ($CDCl_3$) δ 1.44 (s, 9H), 2.63 (s, 3H), 3.95 (s, 3H), 5.79 (br s, 2H), 6.98 (dt, $J = 7.5$, 1.8 Hz, 1H), 7.15 (dt, $J = 8.1$, 1.8 Hz, 1H), 7.24 (t, $J = 7.5$ Hz, 1H); mass spectrometry (TOF) $m/z = 421.1163$ ($M + H^+$) (theoretical 421.1168).

***N*-*tert*-Butyl-5-amino-4-(3-fluorophenyl)-2-(methylthio)thieno-[2,3-*d*]pyrimidine-6-carboxamide (18).** Analysis by C_8 reversed-phase LC−MS using a linear gradient of H_2O with increasing amounts of CH_3CN (0 → 15 min, 45% → 90% CH_3CN at a flow rate of 1 mL/min, $t_R = 11.4$ min) indicated greater than 92% purity by peak integration. ^{1}H NMR ($CDCl_3$) δ 1.54 (s, 9H), 2.68 (s, 3H), 7.19−7.50 (m, 4H); mass spectrometry (TOF) $m/z = 391.1072$ ($M + H^+$) (theoretical 391.1057).

***N*-*tert*-Butyl-5-amino-4-(3-hydroxyphenyl)-2-(methylthio)-thieno[2,3-*d*]pyrimidine-6-carboxamide (19).** Analysis by C_8 reversed-phase LC−MS using a linear gradient of H_2O with increasing amounts of CH_3CN (0 → 10 min, 25% → 90% CH_3CN at a flow rate of 1 mL/min, $t_R = 10.1$ min) indicated greater than 92% purity by peak integration. ^{1}H NMR ($CDCl_3$) δ 1.45 (s, 9H), 2.64 (s, 3H), 5.98 (br s, 2H), 7.02 (d, $J = 7.2$ Hz, 2H), 7.12 (d, $J = 7.5$ Hz, 1H), 7.39 (t, $J = 7.8$ Hz, 1H); mass spectrometry (TOF) $m/z = 389.110$ ($M + H^+$) (theoretical 389.1106).

***N*-*tert*-Butyl-5-(-dimethylamino)-4-(3-methoxyphenyl)-2-(methylthio)thieno[2,3-*d*]pyrimidine-6-carboxamide (20).** Analysis by C_8 reversed-phase LC−MS using a linear gradient of H_2O with increasing amounts of CH_3CN (0 → 5 min, 50% → 90% CH_3CN, 5 → 15 min, 90% CH_3CN at a flow rate of 1 mL/min, $t_R = 7.4$ min) indicated greater than 93% purity by peak integration. ^{1}H NMR ($CDCl_3$) δ 1.43 (s, 9H), 2.37 (s, 6H), 2.63 (s, 3H), 3.84 (s, 3H), 7.03 (d, $J = 8.4$ Hz, 1H), 7.09−7.11 (m, 2H), 7.38 (t, $J = 8.1$ Hz, 1H), 7.48 (br s, 1H); mass spectrometry (TOF) $m/z = 431.1553$ ($M + H^+$) (theoretical 431.1575).

Tissue Culture and cAMP Assay. Cells were cultured for 48 h in 24-well plates before incubation for 1 h in serum-free DMEM containing 1 mM 3-isobutyl-1-methylxanthine (IBMX) (Sigma) and bovine TSH (1.8 μM) (Sigma) or human LH (1000 ng/mL) (Dr. A. Parlow, NIDDK National Hormone and Pituitary Program) or compounds **3**−**19** (0−100 μM) in a humidified 5% CO_2 incubator. Following aspiration of the medium after incubation with compounds, cells were lysed using lysis buffer 1 of the cAMP Biotrak enzyme immunoassay (EIA) system (Amersham Biosciences). The cAMP content of the cell lysate was determined using the manufacturer's protocol. The efficacy of receptor activation by small-molecule modulators is expressed as the percent of maximum response of LHCGR or TSHR to LH or TSH, respectively. The potency (EC_{50}) was obtained from dose−response curves (0−100 μM compound) by data analysis with GraphPad Prism 4 for Windows.

Acknowledgment. The authors thank Dr. John Lloyd and Dr. Sonya Hess for assistance in obtaining HRMS data. Special thanks are given to Amanda Skoumbordis for assistance in editing this manuscript. This work was supported by the Intramural Research Program of the National Institute of Diabetes and Digestive and Kidney Diseases, National Institutes of Health.

Supporting Information Available: Characterization of all synthetic compounds and biological constructs, docking procedures, detailed descriptions of the docking results, and full-page pictures of **3**, **5**, and **7** at the TSHR and LHCGR. This material is available free of charge via the Internet at http://pubs.acs.org.

References

(1) de Roux, N.; Doeker, B.; Milgrom, E. In *Hormone Signaling*; Goffin, V., Kelly, P. A., Eds.; Kluwer Academic Publishers: Norwell, MA, 2002; p 199.
(2) Millar, R. P.; Lu, Z.-L.; Pawson, A. J.; Flanagan, C. A.; Morgan, K.; Maudsley, S. R. Gonadotropin-Releasing Hormone Receptors. *Endocr. Rev.* **2004**, *25*, 235−275.
(3) Szkudlinski, M. W.; Fremont, V.; Ronin, C.; Weintraub, B. D. Thyroid-Stimulating Hormone and Thyroid-Stimulating Hormone Receptor Structure−Function Relationships. *Physiol. Rev.* **2002**, *82*, 473−502.
(4) Cooper, D. S. Drug Therapy: Antithyroid Drugs. *N. Engl. J. Med.* **2005**, *352*, 905−917.
(5) Guo, T. Small Molecule Agonists and Antagonists for the LH and FSH Receptors. *Expert Opin. Ther. Pat.* **2005**, *15*, 1555−1564.
(6) van Straten, N. C. R.; van Berkel, T. H. J.; Demont, D. R.; Karstens, W.-J. F.; Merkx, R.; Oosterom, J.; Schulz, J.; van Someren, R. G.; Timmers, C. M.; van Zandvoort, P. M. Identification of Substituted 6-Amino-4-phenyltetrahydroquinoline Derivatives: Potent Antagonists for the Follicle-Stimulating Hormone Receptor. *J. Med. Chem.* **2005**, *48*, 1697−1700.
(7) Maclean, D.; Holden, F.; Davis, A. M.; Scheuerman, R. A.; Yanofsky, S.; Holmes, C. P.; Fitch, W. L.; Tsutsui, K.; Barrett, R. W.; Gallop, M. A. Agonists of the Follicle Stimulating Hormone Receptor from an Encoded Thiazolidinone Library. *J. Comb. Chem.* **2004**, *6*, 196−206.
(8) van Straten, N. C. R.; Schoonus-Gerritsma, G. G.; van Someren, R. G.; Draaijer, J.; Adang, A. E. P.; Timmers, C. M.; Hanseen, R. G. J. M.; van Boeckel, C. A. A**.** The First Orally Active Low Molecular Weight Agonists for the LH Receptor: Thienopyr(im)idines with Therapeutic Potential for Ovulation Induction. *ChemBioChem* **2002**, *3*, 1023−1026.
(9) Jäschke, H.; Neumann, S.; Moore, S.; Thomas, C. J.; Colson, A.-O.; Costanzi, S.; Kleinau, G.; Jiang, J.-K,; Paschke, R.; Raaka, B. M.; Krause, G.; Gershengorn, M. C. A Low Molecular Weight Agonist Signals by Binding to the Trnasmembrane Domain of Thyroid-Stimulating Hormone Receptor (TSHR) and Luteinizing Hormone/Chorionic Gonadotropin Receptor (LHCGR). *J. Biol. Chem.* **2006**, *281*, 9841−9844.
(10) Kappe, C. O. Recent Advances in the Biginelli Dihydropyrimidine Synthesis. New Tricks from an Old Dog. *Acc. Chem. Res.* **2000**, *33*, 879−888.
(11) The synthesis of *tert*-butyl-2-mercaptoacetate was accomplished via procedures reported by Woulfe and Miller: Woulfe, S. R.; Miller, M. J. The synthesis of substituted [[3(*S*)-(acylamino)-2-oxo-1-azetidinyl]thio]acetic acids. *J. Org. Chem.* **1986**, *51*, 3133−3139. The general procedure involves the addition of potassium ethylxanthate to *tert*-butyl chloroacetate in acetone to afford *O*-ethyl *S*-(*tert*-butoxycarbonyl)methyl dithiocarbonate in 97% yield. Subsequent treatment with ethanolamine provided *tert*-butyl-2-mercaptoacetate in 34% yield.
(12) General experimental procedures and spectroscopic characterization for all intermediates are reported in Supporting Information. A benzyl deprotection was necessary for the complete synthesis of **19**. Additional evaluation of the purity of **3**−**20** was judged by HPLC analysis of individual compounds within two dissimilar mobile phase gradients. A table describing the results is reported in Supporting Information.

(13) Libert, F.; Lefort, A.; Gerard, C.; Parmentier, M.; Perret, J.; Ludgate, M.; Dumont, J. E.; Vassart, G. Cloning, sequencing and expression of the human thyrotropin (TSH) receptor: Evidence for binding of autoantibodies. *Biochem. Biophys. Res. Commun*. **1989**, *165*, 1250−1255.

(14) Schulz, A.; Schoneberg, T.; Paschke, R.; Schultz, G.; Gudermann, T. Role of the Third Intracellular Loop for the Activation of Gonadotropin Receptors**.** *Mol. Endocrinol*. **1999**, *13*, 181−190.

(15) Kleinau, G.; Jäschke, H.; Neumann, S.; Lättig, S.; Paschke, R.; Krause, G. Identification of a Novel Epitope in the Thyroid-Stimulating Hormone Receptor Ectodomain Acting as Intramolecular Signaling Interface. *J. Biol. Chem*. **2004**, *279*, 51590−51600.

(16) Abagyan, R.; Totrov, M.; Kuznetsov, D. ICM. A New Method For Protein Modeling and Design: Applications to Docking and Structure Prediction from the Distorted Native Conformation. *J. Comput. Chem.* **1994**, *15*, 488−506.

(17) Ballesteros, J. A.; Weinstein, H. Integrated Methods for Modeling G-Protein Coupled Receptors. *Methods Neurosci*. **1995**, *25*, 336−428.

(18) Costanzi, S.; Mamedova, L.; Gao, Z.-G.; Jacobson, K. A. Architecture of P2Y Nucleotide Receptors: Structural Comparison Based on Sequence Analysis, Mutagenesis, and Homology Modeling. *J. Med. Chem*. **2004**, *47*, 5393−5404.

JM060247S